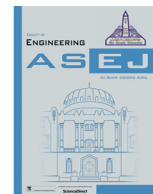




Contents lists available at ScienceDirect

Ain Shams Engineering Journal

journal homepage: [www.sciencedirect.com](http://www.sciencedirect.com)

Architectural Engineering

## Tailored methods for mapping urban heat islands in Greater Cairo Region

Esraa Elmarakby, Marwa Khalifa, Abeer Elshater\*, Samy Afifi

Department of Urban Design and Planning, Faculty of Engineering, Ain Shams University, Egypt



## ARTICLE INFO

## Article history:

Received 9 March 2021

Revised 15 June 2021

Accepted 16 June 2021

Available online 15 July 2021

## Keywords:

Albedo

Ambient air temperature

Egypt

Land surface temperature

LCZs

SPSS

## ABSTRACT

Globally, there is a rapid development of urban heat island (UHI) detection tools, and their results can be accepted regardless of their accuracy in measuring the real impact of the phenomenon. In this study, we investigated various UHI measuring tools and analysed their findings to better interpret their reliability. The tools in the current research adopted remote sensing and field measurements including those using air temperature monitors and thermal imaging technologies to examine the multiple urban structures of four cases in the Greater Cairo Region. The results showed that UHI detection by remote sensing analysis was affected by normalised difference vegetation index. In contrast, field measurements were also influenced by the albedo of morphological materials present. The conclusions revealed that the tools do not provide the same results and indicate that studying UHIs in the built environment differs from investigating it in a two-dimensional layer using remote sensing.

© 2021 THE AUTHORS. Published by Elsevier BV on behalf of Faculty of Engineering, Ain Shams University. This is an open access article under the CC BY-NC-ND license (<http://creativecommons.org/licenses/by-nc-nd/4.0/>).

### 1. Introduction

The urban heat island (UHI) phenomenon occurs when cities replace natural land cover with dense concentrations of pavements, buildings, and other surfaces that absorb and retain heat. It is also a form of air pollution and is the main cause of global warming. UHI increases the temperature of urban areas, such as city centres, compared to that in the surrounding rural and suburban areas [1]. Consequently, this effect increases energy demand in cities [2,3]. In this respect, a considerable amount of literature has been published on global warming and the UHI [4–6]. In addition, UHI is aggravated by climate change [7]. Climate change raises the air temperature [8] and increases the severity of heat waves in

terms of intensity and frequency [5]. Consequently, urban areas that suffer from UHIs bear the brunt of these harsh heat events [9,4].

Previous studies have depended on different methods and tools for measuring UHIs [10–12]. In contrast, many current tools and techniques developed are being used for scientific research regardless of their appropriateness in measuring the UHI phenomenon or defining its limitation, which this study attempted to achieve. No previous studies on UHIs have focused on presenting the differences in the measurement results of various tools [13]. However, each tool can provide different measures for the same area.

This study tackles the challenging problem of the rapid development of UHI detection tools used for credentials, aside from its credibility in measuring the exact effect of the phenomenon. Various tools yield different results in similar cases, and this might require verification of the results to ascertain appropriateness and to help make better judgement. Building on the gap in the literature and the research challenge, we aimed to test the UHI phenomenon using contemporary methods in four areas in the Greater Cairo Region (GCR), Egypt. The purpose was to verify the different measurement results various tools provided in similar-sized areas in metropolitan cities.

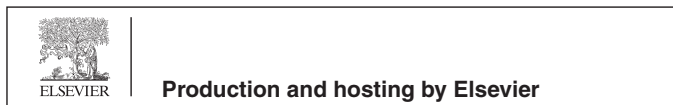
To verify the study materials, four study areas were selected representing the different urban structures of neighbourhoods in GCR: Fatimid Cairo, Garden City, Nasr City, and Alsheroouk City. Similar to previous studies, the cases with different urban forms were chosen to neutralise the urban aspect to ensure the reliability

*Abbreviations:* AAT, Ambient Air Temperature; AST, Average Surface Temperature; DWT, Digital Wireless Thermometer; GCR, Greater Cairo Region; GIS, Geographical Information System; LCZ, Local Climate Zone; LST, Land Surface Temperature; ST, Surface Temperature; NDVI, Normalised Difference Vegetation Index; SPSS, Statistical Package for the Social Sciences (SPSS); UHI, Urban Heat Island.

\* Corresponding author.

E-mail address: [abeer.elshater@eng.asu.edu.eg](mailto:abeer.elshater@eng.asu.edu.eg) (A. Elshater).

Peer review under responsibility of Ain Shams University.



<https://doi.org/10.1016/j.asej.2021.06.030>

2090-4479/© 2021 THE AUTHORS. Published by Elsevier BV on behalf of Faculty of Engineering, Ain Shams University.

This is an open access article under the CC BY-NC-ND license (<http://creativecommons.org/licenses/by-nc-nd/4.0/>).

of the results in the case of contradiction or similarity [14–16]. UHI was estimated using three complementary methods for verification, analysis, and induction, in line with these studies. The study adopted remote sensing techniques, air temperature monitoring devices, and thermal image processing technologies to verify the selected cases.

The added value highlights the contradiction in the results using the three selected methods. The novelty includes applying the measurement methods in the four study areas in the GCR. However, having a limited number of sites for verifying the measurements may require further research.

This study is structured in four sections after this introduction. The first section provides the background for the UHI phenomenon. The second section demonstrates the methods and materials used to perform the empirical study and explains the nature of measurement in the four selected study areas. In the third section, the results showed that applying different tools to the same area for measuring the UHI did not provide the same results, and measuring the phenomenon on the two-dimensional (2D) layer does not reflect the exact effect of the phenomenon. The final section includes the conclusions of the study and highlights areas for future research.

## 2. Background

This section discusses UHI as a phenomenon associated with urbanisation that ends with urban areas in hot temperatures compared to rural and suburban areas [17,18]. The rise in air temperature results in an increase in energy demand, threatening water security [19] and reducing air quality [6].

Several studies have discussed the change in temperature between cities themselves and/or surrounding suburban and rural zones [2,20–22]. This change makes cities hotter owing to the thermal storage capacity of urban structures in urban areas [17,23–25]. Other research argues that the increase in this phenomenon is aggravated by the geographic spread of urban expansion with its constructed surfaces (e.g., roads and rooftops) along with the reduction in green cover and shaded areas [8,26,77].

Studies have examined urban form parameters that affect the increasing or decreasing of local temperature, including urban fabric [27–29]. Other studies tackled surface cover [30,19] and urban structure [4,31,32]. There have been investigations conducted on the UHI phenomenon at the microscale (street canyons) [33–35], local scale (neighbourhood scale), and/or macro-scale (zones/city) [18]. The literature indicates that each scale affects and is affected by the following plate in the hierarchy. The UHI at the local scale is affected by the mesoscale UHI and affects the microscale UHI and vice versa, obeying the theory of part of the whole [4].

Urban expansion, the reduction of vegetation cover, and the arid nature of cities with impervious surfaces such as those of concrete and asphalt, are all the result of rapid urbanisation in many developing countries. These impervious surfaces are the main component of any built environment, and because of their thermodynamic properties, which are different from those of the natural land cover, they alter the energy budget of the planet [36,37]. The UHI is aggravated by the hard and arid surfaces of urban expansion [38].

Some researchers argue that UHIs cause severe impacts, such as the increased demand used in cooling loads, especially at elevated summertime temperatures [2,39,40]. Research has also documented that UHIs threaten water security owing to the high evaporation rate, and UHI raises rainfall temperature, which affects marine life [41,15]. Furthermore, the effects of the increase in daytime temperature that creates a high level of pollution which directly affects human health presents symptoms of general

discomfort [29]. The effect of UHI also causes respiratory difficulties, especially in children, heat cramps, exhaustion, heatstroke, and heat-related mortality [17,18,42–44].

This section has explained that the UHI phenomenon is a global challenge that covers different scales and has consequences. The subsequent section explores the challenge of having precise measurements and results. The procedures and methods for this study are described below.

## 3. Methods and materials

UHIs, a global phenomenon, have been addressed using various measurement tools [45–47]. However, the measuring methods vary in their structures and capabilities to provide specific UHI existence and intensity indicators. As a result, to better investigate the thermal states of the urban envelope, the UHI phenomenon can be assessed using other methods to understand the relationship between the urban structure and the thermal performance [39]. Fig. 1 shows the research methods of analysis and tools investigating the temporal and spatial intensity of the UHI on the local scale of selected sites. The research depended on studying the land surface temperature (LST) and ambient air temperature (AAT) using remote sensing, field measurements, and thermal imaging techniques to obtain a holistic insight into the phenomenon.

### 3.1. Case study

The GCR was selected as the case for this study. It is the largest metropolitan area in Egypt, Africa, and the Middle East, and the world's 17th largest metropolitan city, and the 3rd largest metropolitan area in the Islamic countries besides Jakarta and Karachi [48]. It has a population of approximately twenty-one million inhabitants [49,50]. GCR is subjected to ongoing urban growth due to internal migration and informal urban expansion, which has become the defining features of GCR growth in recent decades [28,51,59,76]. Its diverse urban tissues were also formed during previous eras of its growth [15]. In addition, GCR suffers from an increase in energy demand, with various poverty rates between 0.26% and 91.5% of neighbourhood residents living below the poverty line. Moreover, Egypt is generally threatened by water security issues [52]. The aforementioned factors reinforce the need for UHI studies in GCR [53], as a case of a metropolitan city suffering from the effects of the UHI phenomenon [54].

The GCR heat map showed a distinct thermal pattern associated with the UHI phenomenon. This thermal pattern appeared in the elevated surface temperature (ST) of the urbanised areas, increasing significantly in the condensed urban fabric [8]. Therefore, the sites were chosen for tackling various urban fabrics to separate the influences of urban aspects, and to ensure the credibility of results based on the identification of contrasts and/or similarities. Each study area represented a distinct urban structure of the GCR. For instance, Fatimid Cairo is a clear example of a spontaneous urban pattern, while Garden City represents an organic grid pattern. Additionally, Nasr City can be described as a grid pattern planned city, and Alshrouk City is a hybrid grid.

The local-scale study area was cropped from each location to represent a neighbourhood scale (approximately 0.8 km<sup>2</sup>). Stewart and Oke (1984) [1] classified urban fabrics to facilitate the study of the urban climate in different urban areas. They classified them into ten types under local climate zones (LCZ). The LCZ is a zone of uniform surface cover, including its urban structures, materials, and residents, and extends several kilometres in the horizontal dimension. According to the LCZ classification, the urban structure of the four studied areas varied among compact low-rise, compact mid-rise, compact high-rise, and open low-rise structures in

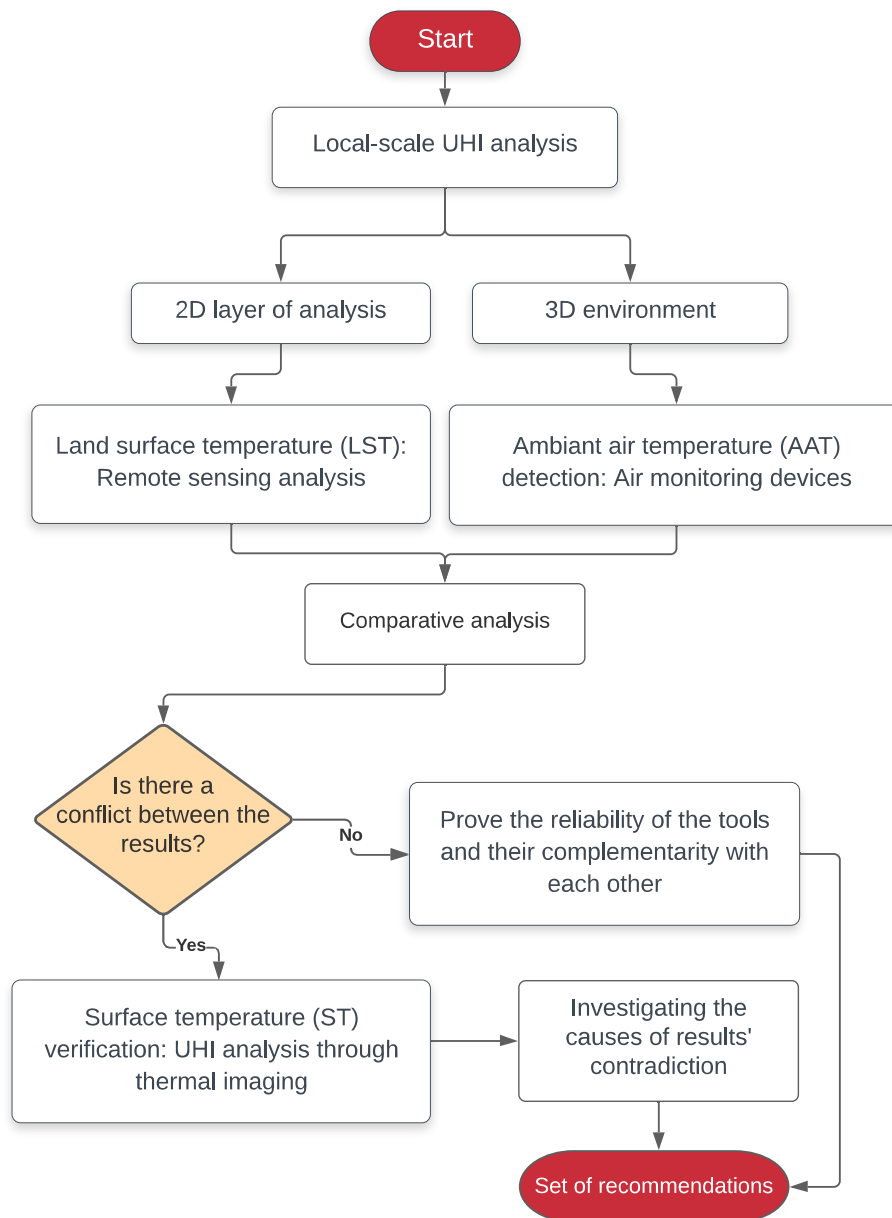


Fig. 1. The research method.

Fatimid Cairo, Garden City, Nasr City, and Alsherouk City, respectively [14], as shown in Fig. 2.

### 3.2. Remote sensing technique

UHI is measured at the local scale using remote sensing techniques based on retrieving the LST and conducting the UHI spatial distribution [46]. Landsat imagery was processed and analysed using remote sensing applications, such as a geographical information system (GIS), to perform this process. In this respect, the present work depended on studying the spatial and temporal distribution of the UHI at a local scale. Analysis of Landsat 8 images was performed in the summer when the UHI was at its peak intensity [47]. The spatial resolution of Landsat 8 is 30 m. This pixel might represent streets, trees, or buildings. Each of these parameters has specific material albedo, distinguished in each study area with streets more expansive than 30 m. However, in the compact irregular urban pattern of Fatimid Cairo, one pixel may have a

value for streets and buildings, as streets are smaller than 30 m. This error was negligible when looking at the streets materials and the structures in Fatimid Cairo, which were interlocking tiles for streets and bricks for buildings. The albedo of the two materials is close (0.3 for bricks and 0.225 for interlocking tiles) [55,56].

Table 1 illustrates the technical details of the analysed satellite images. LST and UHI were detected in the study area. In addition, the normalised difference vegetation index (NDVI) was analysed for the study areas for precise induction of UHI interpretation. NDVI is an indicator for measuring the condition of the vegetation in terms of health and spread, and it is measured using remote sensing depending on the number of reflected lights [57,58]. NDVI has a direct relationship with the UHI. These are inversely correlated [59].

The first step in image processing involves applying the radiometric correction on the thermal bands 10 and 11 using the following formulas [45]:

$$L_{\lambda} = M_L * Q_{cal} + A_L \quad (1)$$

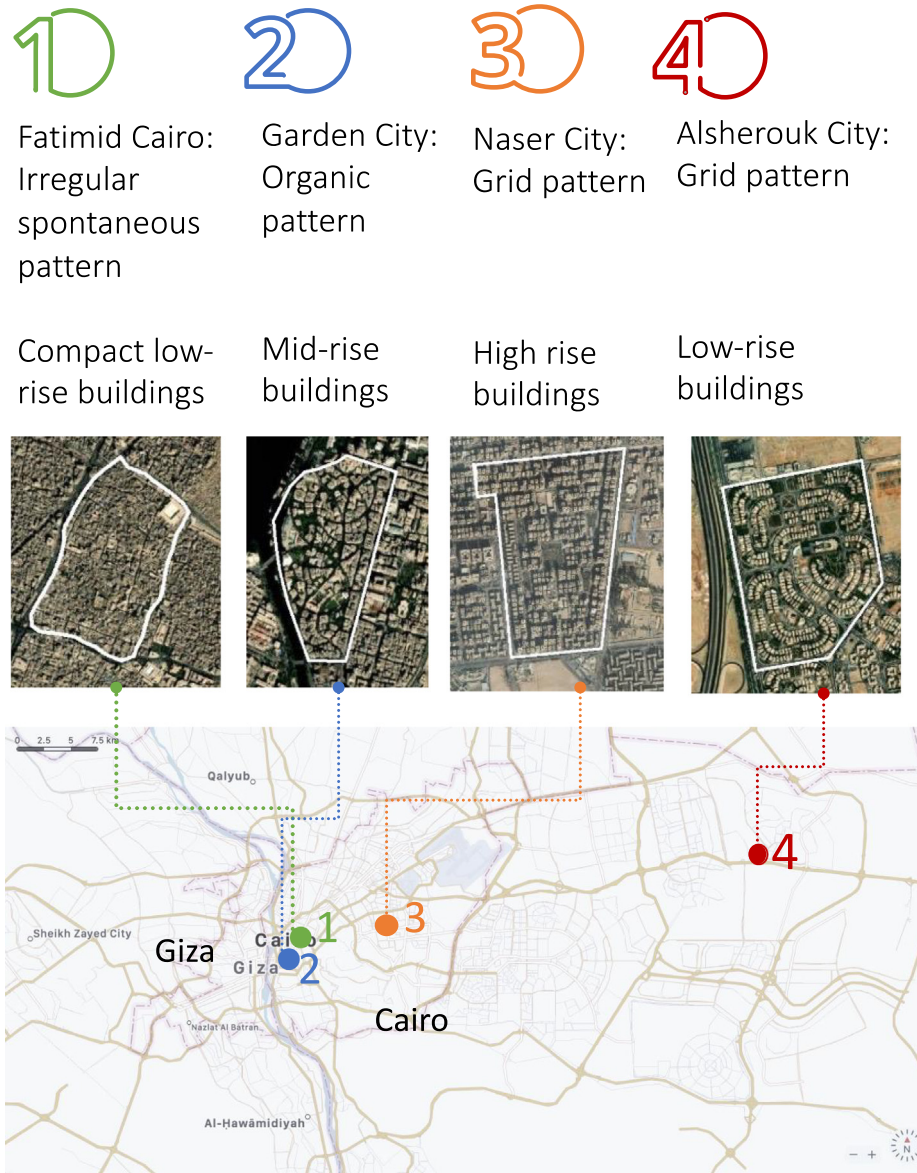


Fig. 2. The four locations of the study areas in GCR.

Table 1  
The Landsat image metadata details.

Season	Satellite	Sensor	Acquisition Time	Path and Row	Spatial resolution*	Cloud Cover
Summer	LandSat 8	OIL_TIRS	20.8.2019	176/39	100	9.54

\* Resolution is resampled to 30 m.

where,  $L_\lambda$  is the spectral radiance (digital numbers) of the images to radiance values ( $W/(m^2 \cdot sr \cdot \mu m)$ ),  $M_L$  is the radiance multiplicative scaling factor,  $A_L$  is the radiance additive scaling factor, and  $Q_{cal}$  is the Landsat band 10 and band 11 [60,61].

$$BT(A^\circ K) = \frac{K_2}{\ln\left(\frac{K_1}{L_\lambda} + 1\right)} \quad (2)$$

where,  $BT$  is the sensor brightness temperature;  $L_\lambda$  is the spectral radiance;  $K_1, K_2$  = thermal conversion constants. The calculated  $BT$  is shown in Kelvin, and to convert it to Celsius degree, the received temperature is added to the absolute zero (approximate =  $-273.15^\circ C$ ).

$$BT(^\circ C) = BT - 273.15 \quad (3)$$

Because of the calibration noises in the Landsat 8 band 11, depending on whether using band 11 in measuring the LST can involve error ratio. In so doing, the mean brightness temperature  $BT_{av}$  was taken as an average between the two analysed bands.

The NDVI was calculated depending on the near infrared band (NIR) and red band [46] as follows:

$$NDVI = \frac{NIR(Band5) - Red(Band4)}{NIR(Band5) + Red(Band4)} \quad (4)$$

where, NDVI is the normalized difference vegetation index.



$$Pv = \left( \frac{NDVI - NDVI_{min.}}{NDVI_{max.} - NDVI_{min.}} \right)^2 \tag{5}$$

The vegetation ( $Pv$ ) proportion reflects the percentage of vegetation occupying the surface in the vertical projection [62].

$$e = 0.004 * Pv + 0.986 \tag{6}$$

After calculating the surface emissivity ( $e$ ), the LST was calculated using the following formula [47]:

$$LST = \frac{BTav}{\left[ 1 + \left( \frac{\lambda_{BT}}{\rho} \right) \ln e \right]} \tag{7}$$

where,  $BTav$  = mean brightness temperature;  $\lambda_{BT}$  = Landsat band 10;  $\rho = (h * C/\sigma)$  where  $h$  is Planck's constant ( $6.626 \times 10^{-34}$  J s),  $C$  is the velocity of the light ( $2.998 \times 10^8$  m/s) 0.01438, and  $\sigma$  is the Boltzmann constant ( $1.38 \times 10^{-23}$  J/K),  $e$  = emissivity.

$$UHI = T \geq 1\sigma + \mu \tag{8}$$

The UHI is the area with a temperature of 1 or more standard deviations above the mean temperature [63].  $\mu$  is the mean LST, and  $\sigma$  is the standard deviation.

### 3.3. Air temperature monitoring

To assess the comprehensive understanding of urban composition influence on UHI at the local scale, local-scale analysis was conducted to study the AAT that the people experience in the urban space [64,65]. Four points were selected in each sample to be monitored using field devices (Table 2) to record the air temperature as the maximum radius for measuring the temperature at a specific point from 100 to 300 m [66]. AAT was measured at each location of the four points in each study area using a digital wireless thermometer (DWT). This device is handheld-portable with an LCD screen that shows temperature and humidity. The accuracy of the appliance was one decimal with an error ratio of 0.001%. The monitoring took place on the same day as the satellite image catching at each study area, from 1:00 pm to 2:00 pm (the peak heat hour) [7,67].

The following formula for measuring LCZ was used to compare the different urban structures and air temperatures measured.

$$\Delta TLCZ = T_{ZONE X} - T_{ZONE Y} \tag{9}$$

where, Zones X and Y represent the two zones where the UHI is calculated as the temperature difference between the two zones.

### 3.4. Thermal image processing

Thermal image analysis was performed for two primary purposes. First, we verified the readings of the local-scale analysis results to validate the remote sensing and field measurement data. Second, we studied the effect of urban materials on the UHI intensity in the ambient environment. Thermal imaging is a technique for studying UHIs that require a very accurate device to be examined, such as high-resolution infrared thermal cameras (FLIR T540) [68]. The thermal imaging camera receives the radiation of a targeted object and the emission from the atmosphere (surrounding radiation on the item) to provide the full thermal states of the captured object [69]. To achieve clear photos, the authors applied the rule of thirds to address the appearance of the three-dimensional environment [70]. The thermal images were captured in the four locations at the field measurement monitoring points using an FLIR T540 Thermal Camera with 24° Lens, 464 × 348 (model: 79302-0201) [69]. The thermal images were processed using FLIR Tools® software [71].



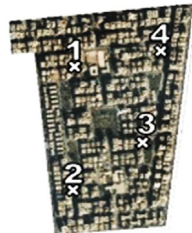

Each site had four addressing issues. First, two shots were taken at each end, representing both sides of the street (365°). The data were collected between 12:00 pm and 3:00 pm on 20 August 2019 and 21 August 2019, which were the same time period for the satellite-captured images with the same urban characteristics for the remote sensing analysis. Third, eight thermal pictures represented each urban form to study their thermal urban characteristics. Fourth, air temperature and relative humidity were also addressed using temperature sensors as required data for image processing. Finally, the correlation between the average surface temperature (AST) retrieved from each scene and the AAT was determined to understand the effect of the surface materials on the UHI [72].

The analysis was based on calculating the temperature difference between the AST and the surface temperature of each urban material. Then,  $\Delta T$  was correlated with the percentage of material presence using the Statistical Package for the Social Sciences (SPSS) to analyse its influence on the thermal warming of urban forms [28,74].

$$\Delta T = \mu_{ST} - T_{Surface Temp} \tag{10}$$

where,  $T$  is the surface temperature (ST) of the urban materials, and  $\mu$  is the mean surface temperature of the scene.

**Table 2**  
The measurement monitoring points.

Location	Fatimid Cairo	Garden City	Nasr City	Alsherouk City
Study area satellite image				
Coordinates	1 30°03'14.4"N 31°15'31.3"E 2 30°02'57.2"N 31°15'28.7"E 3 30°02'59.9"N 31°15'38.0"E 4 30°03'14.6"N 31°15'44.4"E	1 30°02'13.8"N 31°13'49.5"E 2 30°01'59.0"N 31°13'49.3"E 3 30°02'06.6"N 31°13'56.2"E 4 30°02'14.2"N 31°14'00.9"E	1 30°03'09.6"N 31°21'09.8"E 2 30°02'53.8"N 31°21'07.9"E 3 30°03'01.2"N 31°21'18.3"E 4 30°03'13.1"N 31°21'21.6"E	1 30°10'15.5"N 31°35'44.4"E 2 30°10'02.4"N 31°35'57.0"E 3 30°10'18.9"N 31°36'00.5"E 4 30°10'18.9"N 31°36'00.5"E

**Table 3**  
The results from analysing the thermal pattern and the NDVI on the local scale using remote sensing and records of field measurement.

Case Study	Fatimid Cairo (1)	Garden City (2)	Nasr City (3)	Alsherouk City (4)
LST				
UHI				
NDVI				
Ambient Air Temperature detection methods				
Monitoring points	T1 T2 T3 T4	T1 T2 T3 T4	T1 T2 T3 T4	T1 T2 T3 T4
LST	48.7 49.1 49.3 48.6	45.6 45.3 46.2 45.8	45.7 45.6 46.3 46.6	46.4 46.9 47.5 46.8
AAT	38.2 38.6 38.0 38.2	40.2 40.0 40.4 40.3	44.0 44.8 44.1 44.8	39.2 39.0 39.1 39.4
Average LST	48.925	45.725	46.05	46.9
Average AAT	38.25	40.225	44.425	39.175

**4. Results and discussion**

The thermal analysis of the case studies for retrieving the UHIs showed a direct correlation between the LST and the NDVI with a significant coefficient of  $-0.964$ . A decrease in LST followed an increase in NDVI in the studied areas (Table 3). Number one, two, three, and four in horizontal axis in Fig. 3 represent the Fatimid Cairo, Garden City, Nasr City, and Alsherouk City, respectively.

The results indicated that Garden City had 0% of the UHI with an increase in the NDVI values, despite Fatimid Cairo, which was condensed with low NDVI and had 82% UHI density. Nasr City with 18% UHI and Alsherouk City with 29% UHI obeyed the same theory regarding the NDVI. On the local-scale analysis of the UHI, NDVI had a dominant influence on the LST, followed by the albedo values of the materials. The UHI existence in Alsherouk city and Nasr City was derived mainly from the asphalt roads that existed in the UHI

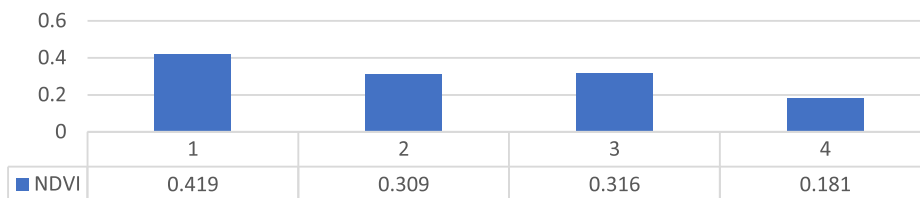


**Fig. 3.** NDVI calculated using remote sensing for the study areas.

**Table 4**  
UHI based on the air temperature records.

Location	Zone	Average AAT	UHI
Fatimid Cairo	1	38.250 °C	$\Delta T Z1-\Delta T Z2 = -1.975$
	2	40.225 °C	$\Delta T Z1-\Delta T Z3 = -6.175$
Garden City	3	44.425 °C	$\Delta T Z1-\Delta T Z4 = -0.925$
Alsherouk City	4	39.175 °C	$\Delta T Z2-\Delta T Z3 = -4.2$
			$\Delta T Z2-\Delta T Z4 = 1.05$
			$\Delta T Z3-\Delta T Z4 = 5.25$

zone as the albedo of the asphalt material was 0.125. Therefore, the absence of NDVI in the Fatimid Cairo zone played a crucial role in representing it as an arid zone with the maximum UHI intensity.

The local-scale field measurements in the four study areas showed different results from the remote sensing analysis. The AAT captured at the four points in each zone recorded the highest air temperature in Nasr City compared to that of Fatimid Cairo, which showed minor AAT records. The UHI was calculated as the magnitude of the temperature difference between LCZ representing each study area. Table 4 and Fig. 4 show the UHI of each study area and its intensity. The research identified Nasr City as the hottest spot that suffered from the UHI compared to Fatimid Cairo with a variance of 3.950 °C.

The thermal imaging analysis conducted on the four study areas ascertained the air temperature results recorded in each zone. AST and AAT were measured and compared to each other on a local scale in each study area, which validated the AAT results on the ST measured using remote sensing data. Studying UHI in a three-dimensional environment is different from looking at it on a 2D layer in remote sensing during the same time of the year, month, and date. The UHI in the remote sensing analysis was affected mainly by the NDVI, while the field measurements in the urban composition were different and influenced by the albedo of the urban structure.

The thermal image provided the advantage of analysing the impact of the materials on the UHI. Each material of the urban envelope was detected, and its temperature was calculated in the four study areas with 16 detection points and 32 thermal images. Figs. 5 and 6 show an example of the thermal images captured using the thermal camera.

The analysis revealed that AAT and AST had a strong relationship with the different urban structures. Considering the above, Nasr City represented the worst case in dealing with the UHI, as its records were the highest among those of the four study areas, followed by Garden City, Alsherouk City, and finally, Fatimid Cairo, which recorded the lowest UHI effect.

The thermal image provided the advantage of analysing the albedo effects on the UHI. However, Fatimid Cairo was the best case with less exposure to UHI, while Alsherouk City had better results than the remaining areas. The emissivity and albedo values were determined for each study area with respect to LST and AST. One of the critical findings was that the urban structure materials

significantly influenced the UHI presence in both the horizontal and vertical dimensions.

The results of the UHI analysis based on thermal imaging ST asserted the existence of AAT in the study areas. These results prove that Nasr City—compact high-rise—was the area most affected by the UHI effect. In the following positions of results, Garden City and Alsherouk City followed Nasr City, and the hierarchy ended with Fatimid Cairo, which was the case of lowest UHI (Fig. 7). The hierarchy was contracted using remote sensing UHI analysis.

Field measurements showed that the metalized vehicle was the most critical urban form exposed to massive heat storage. The results also confirmed that the following influence component was the road asphalt exposed all day to the sun, storing its heat. In the third position of influence, the building material itself was concrete. The fourth was the platforms (e.g., interlock and concrete), and the last one was the green areas which played a significant role in reducing the UHI effect by saving shadows and reflecting heat.

In this work, it is significant that as the presence of heat-absorbing materials increases and the existence of heat-reflective materials decreases, the more urban form becomes prone to UHI on a wide scale. Furthermore, the analysis showed that parameters with different materials, such as asphalt roads and interlock roads, affected the thermal performance of urban composition. Asphalt roads significantly impacted the urban form’s temperature; meanwhile, interlock roads showed a substantially decreased effect. However, concrete buildings stored more heat than the structures of bearing walls. Therefore, the low albedo value and high emissivity rate of some materials could be justified compared to those of others (Fig. 8).

The local-scale analysis using remote sensing and field measurement equipment provided different results and did not provide the same UHI effect. Nevertheless, this represents another side of the phenomenon.

In line with previous studies, it could be said that studying the UHI at different scales (microlocal-meso) using the tools provided in this study is essential to obtain a full image of the phenomenon attitude in the urban form [8,21,54,73,75]. Our results indicated that it is better to use more than one method to analyse the phenomenon as the methods complete each other to formulate the entire perspective of the phenomenon.

Our study has certain limitations. First, this study was limited to investigating the phenomenon on its local scales involving the effect of NDVI, which could be extended for further investigation. Second, the tool used in the present study provided results of UHI effects on LCZs with an overlook for the impact of urban morphology on UHI.

This work provided proof of the solution to the research problem of considering more variable tools when investigating UHI in LCZ. The results lead to the conclusion that no apparent advantage exists in utilizing our methods for analysing UHI effects in various-sized areas.

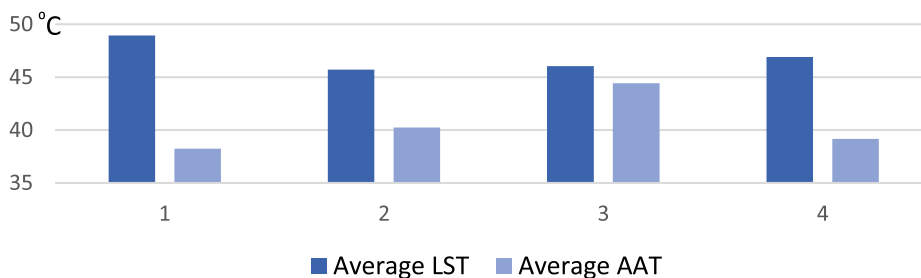


**Fig. 4.** LST retrieved from remote sensing analysis, and the AAT detected using air temperature monitoring devices.

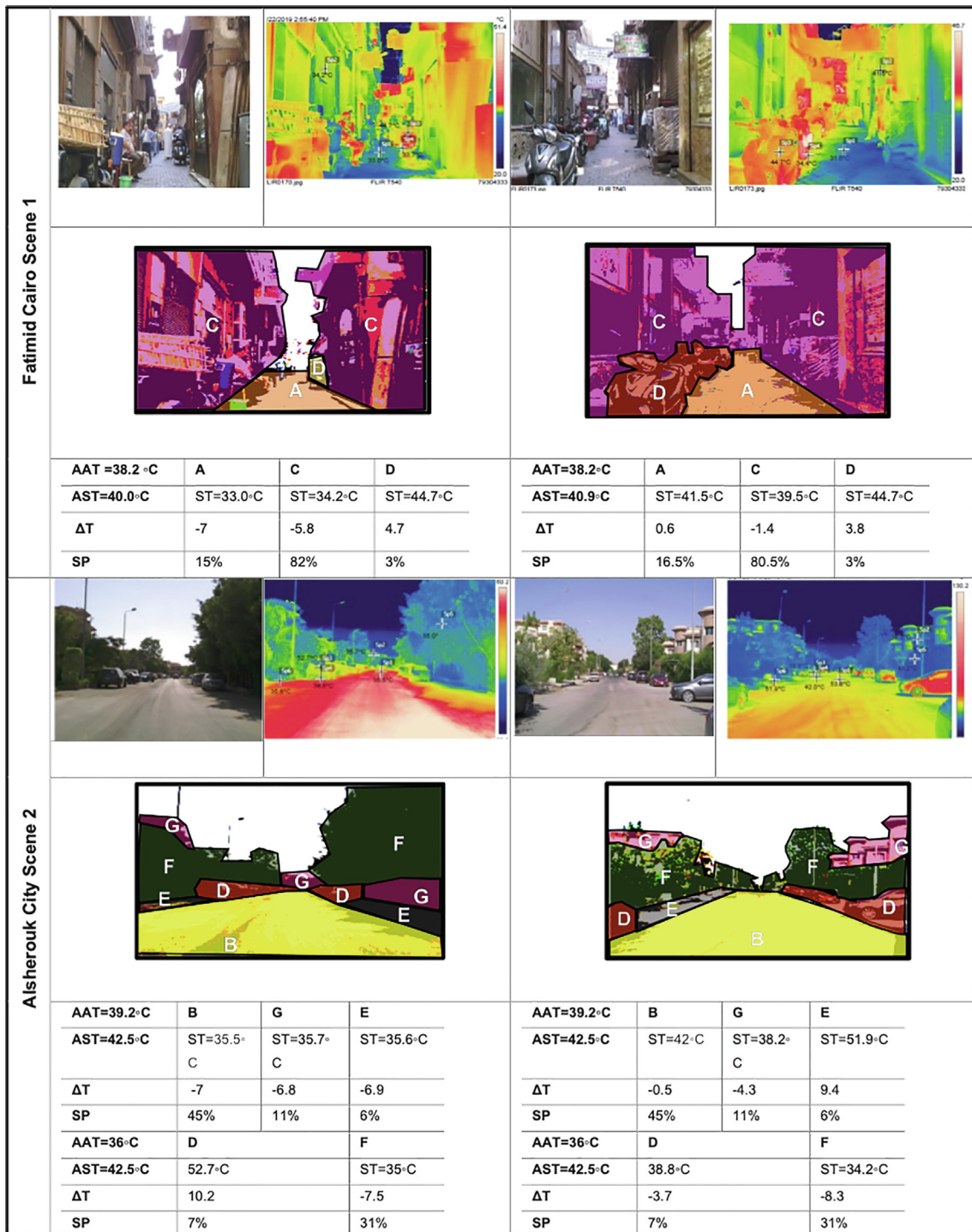


Fig. 5. The thermal images analysis in Fatimid Cairo and Alsheroouk City.



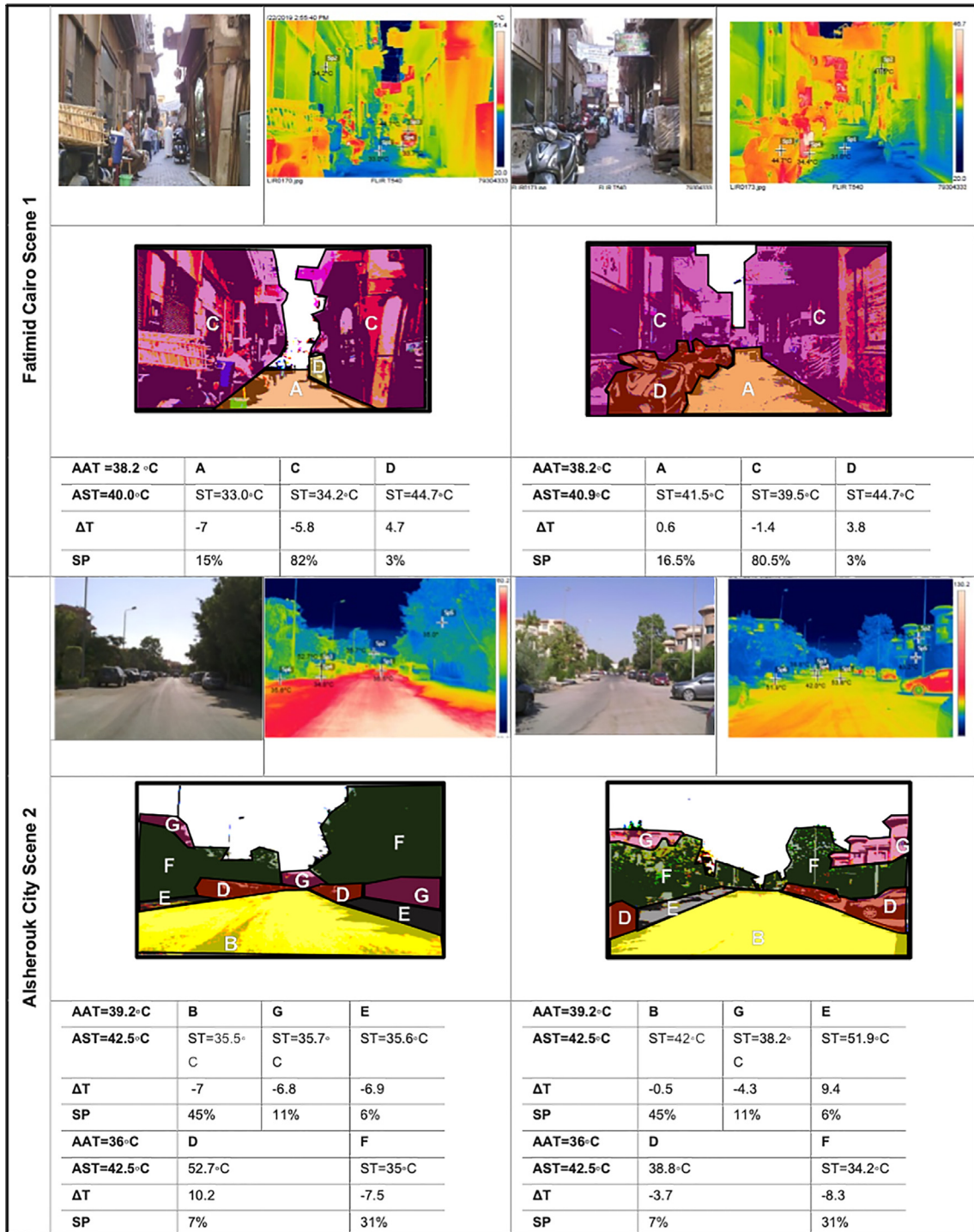


Fig. 6. Analysis of thermal images in Garden City and Nasr City.

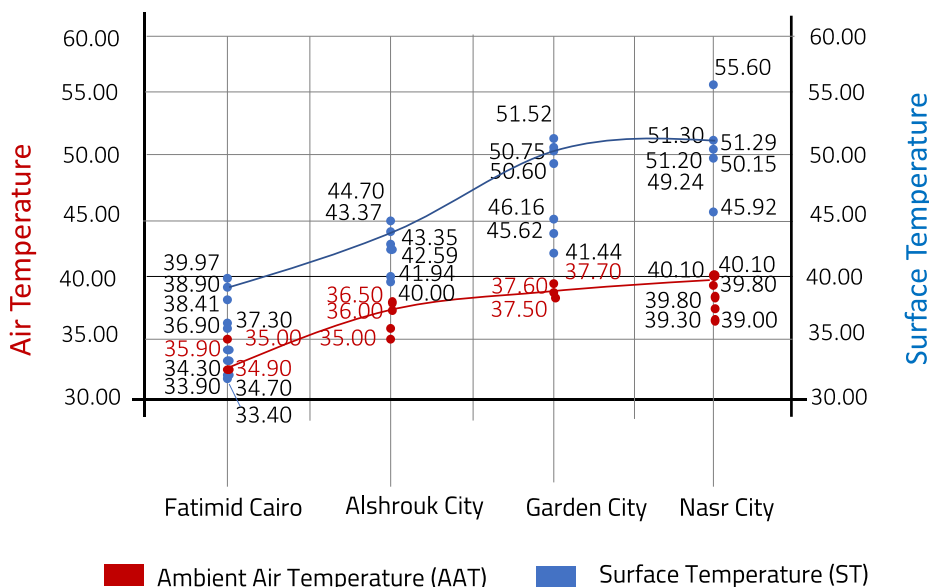


Fig. 7. AAT and ST correlation in the four study areas.

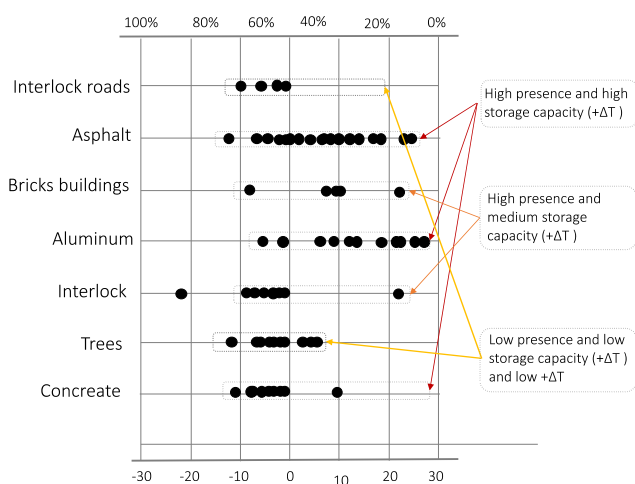


Fig. 8. Influence of the materials on the AST of the urban spaces in the four studied areas.

5. Conclusion

In this study, we investigated the UHIs in four cases in the GCR. Our results indicate that the UHI can be observed using various measurements, methods, and tools. Our data on the four cases were collected using remote sensing, air monitoring devices, and thermal image processing techniques. The results provide evidence that the UHI detection on a 2D layer is different from articulating it in a three-dimensional (3D) environment. NDVI had a crucial influence on the existence of the phenomenon in the 2D layer, as investigated by the remote sensing analysis. At the same time, the albedo of the materials was a significant influencer of the UHI intensity in the 3D environment. Several questions regarding UHI remain to be addressed. A still unsolved question is the verification using measurements in different seasons of the year in studying UHI.

The tool used in the present study provided results of UHI effects on LCZs, but to obtain the whole perspective about the phenomenon, a future study can apply different scales (micro/meso). Subsequently, the correlations between urban morphology param-

eters can be compiled together in future research. Overall, a more systematic and theoretical analysis is required to fully understand the UHI phenomenon, and its spatial and temporal distribution. In addition, as a limited number of comparative studies are available, this study compared four different Cairo areas. Future research could compare the present results with those of other cases of various urban fabrics and consider the potential effects of UHIs in Cairo with a wide number of case studies.

Declaration of Competing Interest

The authors declare that they have no known competing financial interests or personal relationships that could have appeared to influence the work reported in this paper.

Acknowledgements

This paper is based upon work supported by Science, Technology & Innovation Funding Authority (STDF) under grant number [STDF-BARG 37234].

References

- [1] Stewart ID, Oke TR. Local climate zones for urban temperature studies. Bull Am Meteorol Soc 2012;93(12):1879–900. doi: <https://doi.org/10.1175/BAMS-D-11-00019.1>.
- [2] EPA, "Heat Island Impacts," 2018. [Online]. Available: <https://www.epa.gov/heat-islands/heat-island-impacts>.
- [3] Abdallah ASH, Makram A, Nayel MA-A. Energy audit and evaluation of indoor environment condition inside Assiut International Airport terminal building, Egypt. Ain Shams Eng J 2021;2:1–13. doi: <https://doi.org/10.1016/j.asej.2021.03.003>. In press.
- [4] Oke T. Urban climates. Cambridge University Press; 2017.
- [5] Parker J. The Leeds urban heat island and its implications for energy use and thermal comfort. Energy & Buildings 2021;235:1–15. doi: <https://doi.org/10.1016/j.enbuild.2020.110636>.
- [6] Mohajerani A, Bakaric J, Jeffrey-Bailey T. The urban heat island effect, its causes, and mitigation, with reference to the thermal properties of asphalt concrete. Environ Manage 2017;197:522–38. doi: <https://doi.org/10.1016/j.jenvman.2017.03.095>.
- [7] Santamouris M. Recent progress on urban overheating and heat island research. Integrated assessment of the energy, environmental, vulnerability and health impact. Synergies with the global climate change. Energy Build 2020;207:1–28. doi: <https://doi.org/10.1016/j.enbuild.2019.109482>.
- [8] Effat HA, Hassan OAK. Change detection of urban heat islands and some related parameters using multi-temporal Landsat images; a case study for Cairo city,

- Egypt. Urban Clim 2014;10(1):171–88. doi: <https://doi.org/10.1016/j.uclim.2014.10.011>.
- [9] EPA, "Climate Change and Heat Islands," 1 March 2019. [Online]. Available: <https://www.epa.gov/heatislands/climate-change-and-heat-islands> [accessed 5 May 2021].
- [10] Kwon YJ, Lee DK, Kim J-H, Oh K. Improving urban thermal environments by analysing sensible heat flux patterns in zoning districts. *Cities* 2021;116. doi: <https://doi.org/10.1016/j.cities.2021.103276>.
- [11] Acosta MP, Vahdatikhaki F, Santos J, Hammad A, Dorée AG. How to bring UHI to the urban planning table? A data-driven modeling approach. *Sustain Cities Soc* 2021;71. doi: <https://doi.org/10.1016/j.scs.2021.102948>.
- [12] Despini F, Ferrari C, Santunione G, Tommasone S, Muscio A, Teggi S. Urban surfaces analysis with remote sensing data for the evaluation of UHI mitigation scenarios. *Urban Clim* 2021;35:1–12. doi: <https://doi.org/10.1016/j.uclim.2020.100761>.
- [13] Ferreira DG, Diniz CB, Assis ESD. Methods to calculate urban surface parameters and their relation to the LCZ classification. *Urban Climate* 2021;36:1–13. doi: <https://doi.org/10.1016/j.uclim.2021.100788>.
- [14] Elmarakby E, Khalifa M, Elshater A, Afifi S. Spatial morphology and urban heat island: comparative case studies. In: Kamel S, Sabry H, Hassan GF, Refat M, Elshater A, Abd Elrahman AS, et al., editors. *Architecture and Urbanism: A Smart Outlook*. Cham: Springer; 2020. p. 441–54.
- [15] Hassan AAM. Changes in the urban spatial structure of the Greater Cairo Metropolitan area, Egypt, vol. XXXVIII(4); 2011. p. 133–6.
- [16] Racine F. The influence of urban design theories in the transformation of urban morphology: Montreal from 1956 to 2018. *J Urban Des* 2019;24(6):815–39. doi: <https://doi.org/10.1080/13574809.2019.1601994>.
- [17] Oke T. The distinction between canopy and boundary-layer urban heat islands. *Atmosphere* 1976;14(4):268–77. doi: <https://doi.org/10.1080/00046973.1976.9648422>.
- [18] Yin J, Overpeck J, Peyser C, Stouffer R. Big jump of record warm global mean surface temperature in 2014–2016 related to unusually large oceanic heat releases. *Geophys Res Lett* 2018;45:1069–78. doi: <https://doi.org/10.1002/2017GL076500>.
- [19] Steeneveld GJ, Koopmans S, Heusinkveld B, Theeuwes E. Refreshing the role of open water surfaces on mitigating the maximum urban heat island effect. *Landscape Urban Plann* 2014;121:92–6. doi: <https://doi.org/10.1016/j.landurbplan.2013.09.001>.
- [20] Afework B, Hanania J, Stenhouse K, Donev J. Earth's energy budget 18 May 2018. [Online]. Available: [https://energyeducation.ca/encyclopedia/Earth%27s\\_energy\\_budget](https://energyeducation.ca/encyclopedia/Earth%27s_energy_budget).
- [21] Akbari H, Pomerantz M, Taha H. Surfaces and shade trees to reduce energy use and improve air quality in urban areas. *Sol Energy* 2001;70(3):295–310. doi: [https://doi.org/10.1016/S0038-092X\(00\)00089-X](https://doi.org/10.1016/S0038-092X(00)00089-X).
- [22] Sundborg. *Local climatological studies of the temperature conditions*. University of Uppsala; 1950. p. 8.
- [23] Levermore G, Parkinson J, Laycock P, Lindley S. The urban heat island in Manchester 1996–2011. *Build Serv Eng Res Technol* 2015;36(3):343–56. doi: <https://doi.org/10.1177/0143624414549388>.
- [24] Martin-Vide J, Sarricolea P, Moreno-García M. On the definition of urban heat island intensity: the "rural" reference. *Front Earth Sci* 2015;3.
- [25] Gartland L. *Heat islands: understanding and mitigating heat in urban areas*. London: Routledge; 2008.
- [26] Skelhorn C, Ferwati S, Shandas V, Makido Y. Urban form and variation in temperatures. In: *Urban adaptation to climate change: the role of urban form in mediating rising temperatures*. Cham: Springer; 2020. p. 51–73.
- [27] Makido Y, Shandas V, Ferwati S. Predicting urban growth. In: *Urban adaptation to climate change: the role of urban form in mediating rising temperatures*. Cham: Springer; 2020. p. 75–92.
- [28] Elshater A, Abusaada H, Afifi S. What makes livable cities of today alike? Revisiting the criterion of singularity through two case studies. *Cities* 2019;92:273–91. doi: <https://doi.org/10.1016/j.cities.2019.04.008>.
- [29] Abusaada H, Elshater A. Urban design assessment tools: a model for exploring atmospheres and situations. *Proc Inst Civil Eng: Urban Des Plan* 2020;173(6):238–55. doi: <https://doi.org/10.1680/jiurdp.20.00025>.
- [30] Maskooni EK, Hashemi H, Berndtsson R, Arasteh PD, Kazemi M. Impact of spatiotemporal land-use and land-cover changes on surface urban heat islands in a semiarid region using Landsat data. *Int J Digital Earth* 2020. doi: <https://doi.org/10.1080/17538947.2020.1813210>.
- [31] Loutzenheiser D. Pedestrian access to transit: model of walk trips and their design and urban form determinants around bay area rapid transit stations. *Transp Res Rec J Transp Res Board* 1997;1604:40–9. doi: <https://doi.org/10.3141/1604-06>.
- [32] Abusaada H, Elshater A. Revealing distinguishing factors between *Space and Place* in urban design literature. *Journal of Urban Design* 2021;26(3):319–40. doi: <https://doi.org/10.1080/13574809.2020.1832887>.
- [33] Lee H, Mayer H. Solar elevation impact on the heat stress mitigation of pedestrians on tree-lined sidewalks of E-W street canyons – analysis under Central European heat wave conditions. *Urban Forestry & Urban Greening* 2021;58:1–12. doi: <https://doi.org/10.1016/j.ufug.2020.126905>.
- [34] Middel A, Lukaszczuk J, Maciejewski R, Demuzere M. Sky View Factor footprints for urban climate modeling. *Urban Clim* 2018;25:120–34. doi: <https://doi.org/10.1016/j.uclim.2019.100498>.
- [35] Afshari A, Ramirez N. Improving the accuracy of simplified urban canopy models for arid regions using site-specific prior information. *Urban Climate* 2021;35. doi: <https://doi.org/10.1016/j.uclim.2020.100722>.
- [36] Mitchell BC. *Urbanization and Land Surface Temperature in Pinellas County, Florida*; 2011. [Online]. Available: <http://scholarcommons.usf.edu/etd/3250>.
- [37] Habitat UN. *New Urban Agenda, UN Habitat III Conference – United Nations Sustainable Development Goals*. Ecuador: Habitat III; 2017.
- [38] Tiesdell S, Carmona M. *Urban design reader*. 1st ed. Routledge Taylor & Francis Group; 2007.
- [39] Li Y, Schubert S, Kropp JP, Rybski D. On the influence of density and morphology on the Urban Heat Island intensity. *Nat Commun* 2020;11:1–9. doi: <https://doi.org/10.1038/s41467-020-16461-9>.
- [40] Straka M, Sodoudi S. Evaluating climate change adaptation strategies and scenarios of enhanced vertical and horizontal compactness at urban scale (a case study for Berlin). *Landscape Urban Plann* 2019;183:68–78. doi: <https://doi.org/10.1016/j.landurbplan.2018.11.006>.
- [41] EPA, "Heat Island Impacts," 29 July 2020. [Online]. Available: <https://www.epa.gov/heatislands/heat-island-impacts> [accessed 5 May 2021].
- [42] Portier C, Thigpen Tart K, Carter S, Dilworth C, Grambsch A, Gohlke J, et al. *A human health perspective on climate change: a report outlining research needs on the human health effects of climate change*. *Environ Health Perspect* 2010.
- [43] Abusaada H, Elshater A, Abd Elrahman AS. Articulating assemblage theory for salient urban atmospheres in children's environments. *Ain Shams Eng J Arch Eng* 2021;12(2):2331–43. doi: <https://doi.org/10.1016/j.asej.2020.09.021>.
- [44] Elshater A. What can the urban designer do for children? Normative principles of child-friendly communities for responsive third places. *J Urban Des* 2018;23(3):432–55. doi: <https://doi.org/10.1080/13574809.2017.1343086>.
- [45] Al Kuwari N, Ahmed S, Kaiser M. Optimal satellite sensor selection utilized to monitor the impact of urban sprawl on the thermal environment in Doha City, Qatar. *J Earth Sci Climatic Change* 2016;7(1):1–6. doi: <https://doi.org/10.4172/2157-7617.1000326>.
- [46] Li H, Zhou Y, Li X, Meng L, Wang X, Wu S, et al. A new method to quantify surface urban heat island intensity. *Sci Total Environ* 2018;624:262–72. doi: <https://doi.org/10.1016/j.scitotenv.2017.11.360>.
- [47] Zhou B, Lauwaet D, Hooyberghs H, Ridder DR, p. k. Kropp and D. Rybski. Assessing seasonality in the surface Urban Heat Island of London. *J Appl Meteorol Climatol* 2016;55(3):493–505. doi: <https://doi.org/10.1175/JAMC-D-15-0041.1>.
- [48] World Population Review, "Cairo Population 2021 (Demographics, Maps, Graphs)," 17 February 2021. [Online]. Available: <https://worldpopulationreview.com/world-cities/cairo-population>.
- [49] CIA, "Egypt - The World Factbook," 17 February 2021. [Online]. Available: <https://www.cia.gov/the-world-factbook/countries/egypt/>.
- [50] Sutton KFW. Cairo's urban growth and strategic master plans in the light of Egypt's 1996 population census results. *Cities* 2001;18(3):135–49. doi: [https://doi.org/10.1016/S0264-2751\(01\)00006-3](https://doi.org/10.1016/S0264-2751(01)00006-3).
- [51] Sims D, El-Shorbagi Monika, Séjoumé Marion. *Cairo, Egypt. Understanding Slums: Case Studies for the Global Report 2003*. London: UN-HABITAT; 2003. p. 195–228.
- [52] Keyhanpour MJ, Jahromi SHM, Ebrahimi H. System dynamics model of sustainable water resources management using the Nexus Water-Food-Energy approach. *Ain Shams Eng J* 2021;12(2):1267–81. doi: <https://doi.org/10.1016/j.asej.2020.07.029>.
- [53] Tadamun. "Visible Inequality in the Greater Cairo Region: Where the Rich and Poor Live Side-by-Side," 5 2018 August. [Online]. Available: <http://www.tadamun.co/visible-inequality-greater-cairo-region-rich-poor-live-side-side/?lang=en#Yj76LUzZPY> [accessed 5 May 2021].
- [54] Ghoniem E. A remote sensing study of some impacts of global warming on the Arab Region. Boston: Center for Remote Sensing, Boston University; 2009.
- [55] Bradley AV, Thornes JE, Chapman L, Unwin D, Roy M. Modelling spatial and temporal road thermal climatology in rural and urban areas using a GIS. *Climate Res* 2002;22(1):41–55. doi: <https://doi.org/10.3354/cr022041>.
- [56] Hassan M. Evaporation estimation for Lake Nasser based on remote sensing technology. *Ain Shams Eng J* 2013;4(4):593–604. doi: <https://doi.org/10.1016/j.asej.2013.01.004>.
- [57] Ramzi AI. Evaluation feature extracting from DubaiSat-2 satellite images over planned/unplanned complex study area in Egypt. *Ain Shams Eng J* 2018;9(4):3371–9. doi: <https://doi.org/10.1016/j.asej.2018.03.007>.
- [58] Aslam B, Maqsoom A, Alaloul WS, Musarat MA, Jabbar T, Zafar A. Soil erosion susceptibility mapping using a GIS-based multi-criteria decision approach: Case of district Chitral, Pakistan. *Ain Shams Eng J* 2021;12(2):1637–49. doi: <https://doi.org/10.1016/j.asej.2020.09.015>.
- [59] Bek MA, Azmy N, Elkafrawy S. The effect of unplanned growth of urban areas on heat island phenomena. *Ain Shams Eng J* 2018;9(4):3169–77. doi: <https://doi.org/10.1016/j.asej.2017.11.001>.
- [60] Liu L, Zhang Y. Urban Heat Island analysis using the Landsat TM Data and ASTER Data: a case study in Hong Kong. *Remote Sensing* 2011;3(7):1535–52. doi: <https://doi.org/10.3390/rs3071535>.
- [61] Rendenieks Z, Nita MD, Nikodemus O, Radeloff VC. Half a century of forest cover change along the Latvian-Russian border captured by object-based image analysis of Corona and Landsat TM/OLI data. *Remote Sens Environ* 2020;249:1–14. doi: <https://doi.org/10.1016/j.rse.2020.112010>.
- [62] Salimi KH, Sahebi MR, Abkar AA, Zoej M. Fractional vegetation cover estimation in urban environments. *Int Arch Photogrammetry, Remote Sensing Spatial Inform Sci* 2013;XL-1:357–60.
- [63] CCVA. *Urban Heat Island Protocol for Mapping Temperature Projections*. Kleinfelder, City of Cambridge; 2015.

- [64] Yin Y, Tonekaboni NH, Grundstein A, Mishra DR, Ramaswamy L, Dowd J. Urban ambient air temperature estimation using hyperlocal data from smart vehicle-borne sensors. *Comput Environ Urban Syst* 2020;84:1–11. doi: <https://doi.org/10.1016/j.compenurbysys.2020.101538>.
- [65] Watkins R, Palmer J, Kolokotroni M. Increased temperature and intensification of the urban heat island: implications for human comfort and urban design on *JSTOR*. 1st ed., vol. 33. Built Environment, Alexandria Press. <https://www.jstor.org>. *Built Environ* 2007;33(1):85–96.
- [66] Pearce JA, Valvano J, Emelianov S. *Temperature measurements*. Berlin: Springer Netherlands; 2011. p. 399–453. doi:10.1007/978-90-481-8831-4\_11.
- [67] Somers K, Bernhardt E, McGlynn B, Urban D. Downstream dissipation of storm flow heat pulses: a case study and its landscape-level implications. *J Am Water Resour Assoc* 2016;52(2):281–97. doi: <https://doi.org/10.1111/1752-1688.12382>.
- [68] Lee S, Moon H, Choi Y, Yoon DK. Analyzing thermal characteristics of urban streets using a thermal imaging camera: a case study on commercial streets in Seoul, Korea. *Sustainability* 2018;10(2):1–21. doi: <https://doi.org/10.3390/su10020519>.
- [69] FLIR. FLIR T540 Professional Thermal Camera-FLIR Systems; 2018. [Online]. Available: <https://www.flir.com/products/t540/>.
- [70] Elshater A. The power of photography in urban design discipline: a Module Catalogue. *Archnet-IJAR* 2018;12(2):182–208.
- [71] Teledyne FLIR LLC. Thermal Analysis and Reporting (Desktop) FLIR Tools; 2021. [Online]. Available: <https://www.flir.com/products/flir-tools/>. [accessed 2020].
- [72] Kumar S, Mullick SC. Glass cover temperature and top heat loss coefficient of a single glazed flat plate collector with nearly vertical configuration. *Ain Shams Eng J* 2012;3(3):299–304. doi: <https://doi.org/10.1016/j.asej.2012.03.008>.
- [73] Abusaada H, Elshater A. Competitiveness, distinctiveness and singularity in urban design: a systematic review and framework for smart cities. *Sustainable Cities and Society* 2021;68:1–12. doi: <https://doi.org/10.1016/j.scs.2021.102782>.
- [74] El-Metwally Y, Khalifa M, Elshater A. Quantitative study for applying prospect-refuge theory on perceived safety in Al-Azhar Park, Egypt. *Ain Shams Eng J* 2021:1–14. doi: <https://doi.org/10.1016/j.asej.2021.04.016>. In press.
- [75] Abusaada H. Strengthening the affectivity of atmospheres in urban environments: the toolkit of multi-sensory experience. *Archnet-IJAR* 2020;14(3):379–92. doi: <https://doi.org/10.1108/ARCH-03-2020-0039>.
- [76] Khalifa M. Evolution of informal settlements upgrading strategies in Egypt: From negligence to participatory development. *Ain Shams Engineering Journal* 2015;6(4):1151–9. doi: <https://doi.org/10.1016/j.asej.2015.04.008>.
- [77] Abdulateef MF, Al-Alwan HAS. The effectiveness of urban green infrastructure in reducing surface urban heat island. *Ain Shams Engineering Journal* 2021:1–18. doi: <https://doi.org/10.1016/j.asej.2021.06.012>.

**Esraa Elmarakby** is a lecturer assistant in the Department of Urban Design and Planning, Faculty of Engineering, Ain Shams University. She held a Master of Science

in 2020 from Ain Shams University. In her scientific thesis, she examined the effect of the urban context on climate change, focusing on the Urban Heat Islands phenomenon. Esraa is working on a research project funded by the Research, Technology, and Innovation Authority (STDF) [grant number: STDF-BARG 37234]. Esraa has participated in many local and international scientific conferences and workshops on climate change and has published scientific research on climate change and its impact on urbanisation.

**Marwa Khalifa** has obtained her B.Sc. (1995) & M.Sc. (2000), “Urban Planning” specialization from Ain Shams University (ASU), Egypt while her PhD (2007) was a joint supervision from ASU and the University of Sheffield, UK. Currently, Prof. Khalifa acts as a Director of the Graduate Engineering School for Research (GESR) and a coordinator for two programs: B.Sc “Environmental Architecture & Urbanism” (ENVR) and the Interdisciplinary Master on “Resource Efficient Cities” (IMaREC), in addition to being a Professor in the Department of Urban Design & Planning, where she joined the academic staff since 1996. Prof. Khalifa has major interest in informal settlements upgrading, participatory planning approaches, environmental assessment & risk reduction, climate change adaptation, and resource efficient cities. Since 2007 she has participated in and coordinated three international cooperation projects with partner universities in EU, Latin America, South Asia, Africa and the MENA Region related to higher education reform in the fields of participatory planning and natural resources management.

**Abeer Elshater** is a professor of Urban Morphology at Ain Shams University (ASU), Cairo, Egypt, teaching and supervising multidisciplinary topics in the ideology of urban design. She is a personal investigator to a funded research project supported by Research, Technology, and Innovation Authority (STDF), [grant number: STDF-BARG 37234] by Science, Technology and Innovation Funding Authority (STDF) about urban heat islands and urban forms. Elshater has also worked on some international research projects with international universities. She also is co-editor, author and co-author of several books and scientific manuscripts. Currently, Elshater acts as an ambassador of the Regional Studies Association, United Kingdom (UK).

**Samy Afifi** is an assistant professor at the Department of Urban Planning and Design, Faculty of Engineering, Ain Shams University. He is a member of a team responsible for teaching many courses such as Theories and history of urban planning, urban economics, city planning and housing, and computer applications for urban planning. In Professional practice, Samy is a co-founder of the Urban Development Centre. His professional career allowed him to act, discuss, negotiate and deal with a spectrum of people with different backgrounds and governmental organisations all over Egypt. His primary interest is in tracing and analysing dynamics during the evolution of traditional and contemporary urban settlements.